Micro-Raman and micro-infrared spectroscopic studies of Pb- and Au-irradiated $ZrSiO_4$: Optical properties, structural damage, and amorphization

Ming Zhang,[1,*] Lynn A. Boatner,[2] Ekhard K. H. Salje,[1] Rodney C. Ewing,[3] Philippe Daniel,[4] William J. Weber,[5] Yanwen Zhang,[5] and Ian Farnan[1]

[1]*Department of Earth Sciences, University of Cambridge, Downing Street, Cambridge CB2 3EQ, United Kingdom*

[2]*Materials Science and Technology Division, Oak Ridge National Laboratory, Oak Ridge, Tennessee 37831-6056, USA*

[3]*Department of Geological Sciences, University of Michigan, Ann Arbor, Michigan 48109-1005, USA*

[4]*Laboratoire de Physique de l'Etat Condensé (LPEC), UMR CNRS 6087, Université du Maine-Faculté des Sciences, Avenue Olivier Messiaen–72085 Le Mans Cedex 9, France*

[5]*Pacific Northwest National Laboratory, P.O. Box 999, Richland, Washington 99352, USA*

(Received 10 October 2007; revised manuscript received 24 January 2008; published 22 April 2008)

The optical properties of damaged periodic and aperiodic domains created by Pb^+ (280 keV) and Au^{4+} (10 MeV) implantation of zircon were studied using micro-infrared (IR) and micro-Raman spectroscopy. The Pb^+ and Au^{4+} irradiations caused a dramatic decrease in the IR reflectivity similar to that observed for metamict natural zircon. The irradiation with 10 MeV Au^{4+} ions (to fluences of 1×10^{15} Au^{4+} ions/cm^2) also results in the formation of an amorphized phase similar to that observed in metamict zircon. These results show that high-energy, heavy-ion irradiations provide a good simulation of the ballistic effects of the recoil nucleus of an alpha-decay event and, in both cases, the result is the creation of aperiodic domains. Additional IR and Raman features were recorded in samples irradiated with 280 keV Pb^+ ions (to fluences of 1×10^{14} and 1×10^{15} Pb^+ ions/cm^2), indicating the formation of an irradiation-induced additional phase(s). The frequencies of the features are consistent with lead silicates, ZrO_2, and SiO_2. The results show that spectral features of the Au^{4+}- and Pb^+-irradiated zircon are different from those of quenched $ZrSiO_4$ melts, and the finding further confirms that the amorphous state produced by high-energy ion irradiations is structurally different from the glassy state that results from quenching a high temperature melt. In contrast to significant changes in the frequency and width of the Raman ν_3 band observed in metamict zircon, the Pb^+ and Au^{4+} irradiations do not cause similar variations, indicating that the remaining zircon crystalline domains in irradiated samples have a crystalline structure with fewer defects than those of metamict zircon.

DOI: 10.1103/PhysRevB.77.144110 PACS number(s): 61.80.−x, 63.50.−x, 63.20.−e

I. INTRODUCTION

Zircon ($ZrSiO_4$, $I4_1/amd$) is of great interest in the fields of materials science, mineralogy, and geochemistry mainly because of its high chemical stability and durability. Zircon is widely used in the ceramic, foundry, welding-rod coating, and refractory industries. In the geosciences, zircon is the principal phase used in U/Th/Pb age dating because it can incorporate trace amounts of actinides (100–1000s ppm). Accordingly, zircon has been proposed as a phase for the immobilization and disposition of actinides, such as the Pu from dismantled nuclear weapons.[1–6]

Radiation effects caused by the alpha decay of incorporated actinides, whether due to U and Th in natural zircon or Pu in zircon used as a nuclear waste form, have been the subject of extensive studies during the past decades (see Refs. 4 and 7–10 for reviews). Four different approaches have been used in these studies of radiation-induced amorphization and recrystallization of zircon, i.e., (1) investigation[11–43] of the local structure and the damage and recrystallization processes of natural zircons, which have been damaged to varying degrees by the alpha-decay events in the decay chains of incorporated ^{235}U, ^{238}U, and ^{232}Th in the crystals (this natural radiation-damage process in minerals is commonly referred to as metamictization, and the affected material is therefore described as metamict); (2) characterization[19,44–51] of the changes observed in synthetic zircon doped with highly active actinides, such as ^{239}Pu and ^{238}Pu; (3) investigations[52–63] of the damage accumulation and amorphization processes in synthetic and natural zircon irradiated by high-energy ions (e.g., He^+, Xe^+, Kr^+, and Pb^+); and (4) theoretic modelling[64–78] of the damage and recovery processes. These previous investigations elucidated some aspects of the mechanism and kinetics of radiation-damage, amorphization, the recrystallization of metamict zircon, and the nature of the radiation-damage process over different lengths and temporal scales. All of these methods are required in order to develop a full and systematic understanding of the development of the microstructure of zircon as a function of increasing levels of radiation damage over a range of temperature.

The present study is designed to address the following three major questions: What is the structure of the aperiodic domains that result from high-energy irradiations? In fact, there is a limited understanding of the relation between this structure and measured vibrational modes of the aperiodic or amorphous domains produced by the irradiation of zircon. Second, are the aperiodic domains that result from high-energy irradiations the same as those that result from alpha-decay events in natural metamict zircon? The spectral features of each of these types of irradiations will allow for a determination of the similarities and differences between these aperiodic domains created by two very different types of irradiation. These results will provide a basis for evaluat-

ing the extent to which high-energy irradiations can be used to simulate damage from alpha-decay events. Third, are the aperiodic structures created by high-energy irradiations the same as the structure of an amorphous material quenched from a melt, as previous studies[79] report significant spectral differences?

II. EXPERIMENT

The starting materials used for Pb^+ irradiation were pure, synthetic zircon crystals that were grown by means of a high-temperature solution (flux) technique.[80] The Pb implantation was carried out at Oak Ridge National Laboratory. The as-grown $ZrSiO_4$ single crystals were mounted in an Extrion ion implantation accelerator for implantation with Pb^+ ions at an energy of 280 keV at 1×10^{13}, 1×10^{14}, and 1×10^{15} ions/cm^2, respectively. The lead ions were generally implanted near the (110) or cleavage faces, but with an alignment of the Pb^+ beam $\sim15°$ off of this direction in order to avoid ion channelling effects during the implantation process, which at the highest fluence produced a damage layer extending to about 100 nm into the sample from the surface. The sample used for Au^{4+} irradiation was a polycrystalline ceramic zircon. For the preparation of the ceramic, fine grained quartz (SiO_2) and baddeleyite (ZrO_2) were milled in an oscillatory ball mill and pressed into a pellet. The pellet was fired at 1673 K overnight. High-sensitivity ^{29}Si NMR detected $\sim0.5\%$ amorphous SiO_2 in the final sample. The pellet was sectioned and polished into a 2×10 mm^2 ~200-μm-thick specimen. A 10 MeV Au ion beam was rastered over the entire specimen surface at a temperature of 190 K to a total fluence of 1×10^{15} ions/cm^2, using the ion accelerator facility at Pacific Northwest National Laboratory. The Au irradiation at 190 K reduced the dose necessary for amorphization and produced a thick amorphous region that extended from the surface to a depth of about 2 μm. The use of this irradiated ceramic zircon for the present study is mainly due to its availability and also because the sample is irradiated with an ion that is different from Pb^+. Three natural metamict zircon crystals (with f, the fraction of the amorphous phase, of ~0.4, ~0.6, and ~1.0; f was determined using the spectroscopic method reported previously[81]) from Sri Lanka, whose structure is partially or highly damaged by alpha-decay events, and three high-pressure shocked zircon samples (all of which were originally crystalline zircon; two were experimentally shocked at 20 and 38 GPa, respectively, using the shock reverberation technique reported by Deutsch and Schärer,[82] and one was shocked at 83 GPa to fully transform it to reidite[83]—a high-pressure polymorph of zircon) were analyzed for comparison. In addition, powders of PbO, PbO_2, Pb_3O_4, and $PbZrO_3$ from Aldrich were also measured for comparison and to check for the presence of Pb-related phases.

An infrared microscope (IR OPUS-II) equipped with a mapping stage and attached to a Bruker IFS 113v Fourier transform (FT) infrared spectrometer was used to record reflection spectra between 650 and 5000 cm^{-1} at an almost normal incident condition (with a 36× objective) and at a grazing angle of 80° (using an 80° Bruker grazing angle objective). A liquid-nitrogen-cooled narrow-band mercury cadmium telluride detector, coupled with a KBr beam splitter and a Globar source, was used. All of the micro-infrared data in the present study were recorded under unpolarized conditions. Au mirrors were used as references in the reflectance measurements. The measured area has a diameter of 20–60 μm. The final spectra were averaged over 1000 scans with an instrumental resolution of 2 cm^{-1}.

Confocal Raman spectra of the $ZrSiO_4$ samples were recorded in a backscattering configuration by using a T64000 Jobin-Yvon ISA multichannel Raman spectrometer [coupled with an Olympus FX40 microscope and a liquid-nitrogen-cooled charge coupled device (CCD) detector] and a LabRam micro-Raman spectrometer (coupled with a room-temperature CCD detector and a free-sample-space Olympus microscope). A confocal pinhole conjugated with the microscope was adjusted to values that would enhance the experimental resolution. A triple subtractive configuration (gratings of 1800 lines/mm) of the T64000 spectrometer was selected in order to improve the resolution. The 568, 514, and 488 nm excitation laser lines (coherent argon-krypton ion laser) and the 632 nm (Ne-He laser) were used in order to check possible luminescence and fluorescence signals. Slit widths were adjusted to obtain an instrumental resolution of 2 cm^{-1}. The data recording was mainly carried out using a 100×-magnification objective (the use of 100×-magnification objectives gave a beam size of 1–2 μm), although test runs were also done using a 50×-magnification objective. Laser power was carefully chosen to avoid potential damage to the measured areas caused by the intense local heat from the laser beam. Levels of 1 and 30 mW were tested with the 100×-magnification objective, and the low power levels were used. The time dependence of Raman spectra showed no indication of surface damage caused by the laser radiation. Raman depth measurements (sampling points from the surface to 30 μm deep into the bulk) were also completed. For Raman measurements of other Pb-related materials, FT-Raman spectra were recorded at room temperature by using a Bruker FRA 106 FT-Raman accessory attached to a Bruker IFS 66v spectrometer since some of the specimens are colored. A silicon-coated calcium fluoride beam splitter and an excitation radiation of 1064 nm from a Nd:YAG (where YAG denotes yttrium aluminum garnet) laser (which can produce a 350 mW output) and a liquid-nitrogen-cooled high-sensitivity Ge detector were used for the FT-Raman measurements. The spectra were recorded with a backscattering geometry and an instrumental resolution of 2 cm^{-1}. For crystalline zircons, 250–512 scans were completed; 1000–3000 scans were employed for the heavily damaged zircons.

III. RESULTS

Zircon is tetragonal ($I4_1/amd$ or D_{4h}^{19}). Group theory[84] predicts the irreducible representations at $\boldsymbol{k}=0$ for the D_{4h}^{19} space group as follows:

$$\Gamma = 2A_{1g} \oplus A_{2g} \oplus 4B_{1g} \oplus B_{2g} \oplus 5E_g \oplus A_{1u} \oplus 4A_{2u} \oplus B_{1u} \oplus 2B_{2u} \oplus 5E_u.$$

A_{2u} and E_u are IR active, and A_{1g}, B_{1g}, E_g, and B_{2g} are Ra-

TABLE I. A group-theoretical analysis of the internal vibrations in zircon. Raman data are from this study and infrared data from Zhang and Salje (Ref. 81). (Note: R=Raman active, IR=infrared active, and S=optically silent.)

T_d Free SiO_4	D_{2d} Site group	D_{4h} Factor group	$ZrSiO_4$ (cm^{-1})
ν_1 (A_1)	A_1	A_{1g} (R)	975
		B_{2u} (S)	silent
ν_2 (E)	A_1	A_{1g} (R)	439
		B_{2u} (S)	silent
	B_1	B_{2g} (R)	266
		A_{1u} (S)	silent
ν_3 (F_2)	B_2	B_{1g} (R)	1008
		A_{2u} (IR)	980
	E	E_g (R)	923
		E_u (IR)	880
ν_4 (F_2)	B_2	B_{1g} (R)	641
		A_{2u} (IR)	606
	E	E_g (R)	545
		E_u (IR)	431

man active, while A_{2g}, A_{1u}, B_{1u}, and B_{2u} are optically silent. Because the SiO_4 group (D_{2d}) in zircon can be treated as isolated and the modes of the SiO_4 group can be considered as internal modes,[84] the infrared and Raman modes can be simplified as two acoustic modes ($A_{2u} \oplus E_u$), six translatory external modes ($2B_{1g} \oplus 2E_g \oplus A_{2u} \oplus E_u$), four rotation external modes ($A_{2g} \oplus E_g \oplus B_{1u} \oplus E_u$), and 14 internal modes ($2A_{1g} \oplus 2B_{1g} \oplus B_{2g} \oplus 2E_g \oplus A_{1u} \oplus 2A_u \oplus 2B_{2u} \oplus 2E_u$). Table I lists the assignments for the observed internal modes related to the SiO_4 groups.

A. Micro-infrared spectra of Pb- and Au-irradiated zircon

Spectral variations in the micro-infrared spectra of Pb^+-irradiated zircon crystals are shown in Figs. 1 and 2. The spectra in this region are due to stretching vibrations from SiO_4 groups (Table I), which have been shown to be sensitive to radiation damage.[81] The spectra exhibit changes in three aspects: a decrease in reflectivity or IR intensity, a change in spectral pattern, and the occurrence of new features. With increasing irradiation fluence, the crystal irradiated to a fluence of 1×10^{14} Pb ions/cm^2 has a reflectivity (near 980 cm^{-1}) that is only half the value of that from the crystalline or unirradiated crystal and the crystal irradiated to the lowest dose (10^{13} Pb^+/cm^2). The reflectivity dramatically decreases with an increased fluence of 1×10^{15} Pb^+ ions/cm^2. We explain this change as being due to the irradiation-induced damage in zircon and the formation of amorphous domains. These amorphous areas in zircon are expected to have a much lower reflectivity, as well as a low absorptivity, in the frequency region as previously shown by IR work[20,81,85] on metamict zircon. The change in the spectral patterns mainly occurs in crystals irradiated at 1×10^{14} and 1×10^{15} Pb^+ ions/cm^2. As shown in Fig. 1, the undamaged zircon has main reflectance features between 900 and 1100 cm^{-1}, but the pattern is significantly modified

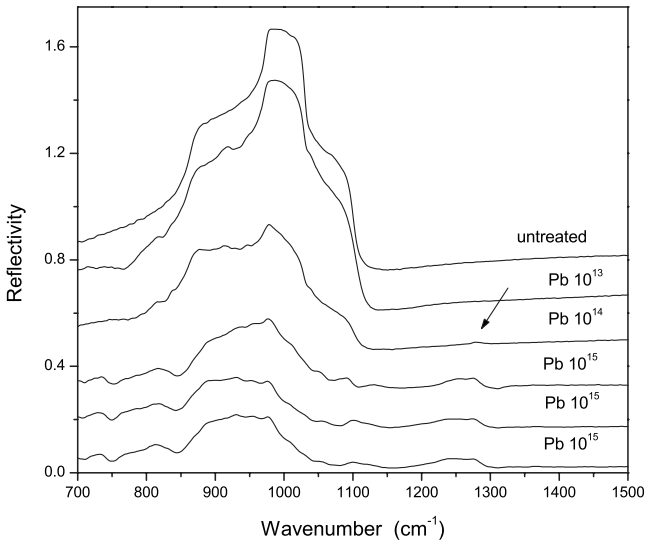

FIG. 1. Micro-infrared reflectance spectra of Pb^+-irradiated zircon with doses of 1×10^{13}, 1×10^{14}, and 1×10^{15} Pb^+ ions/cm^2. For the dose of 1×10^{15} Pb^+ ions/cm^2, two more spectra taken in different spots are also included to illustrate variations in the local structure.

in the crystal irradiated at 1×10^{15} Pb^+ ions/cm^2. The Pb^+-irradiated crystals show IR spectra that are different from that of highly metamict zircon (with f of ~1.0) (Fig. 3), although features of the latter seem to contribute to the broad background of the former (as indicated by the dash line in Fig. 3). The Pb^+ irradiation produces some additional features that are absent in undamaged zircon. For example, there are extra bands near 730 and 1100 cm^{-1}, and broad features occur between 760 and 850 cm^{-1} and between 1200 and 1300 cm^{-1} for the crystal irradiated to a fluence of 1×10^{15} Pb ions/cm^2. The feature near 730 cm^{-1} is assigned

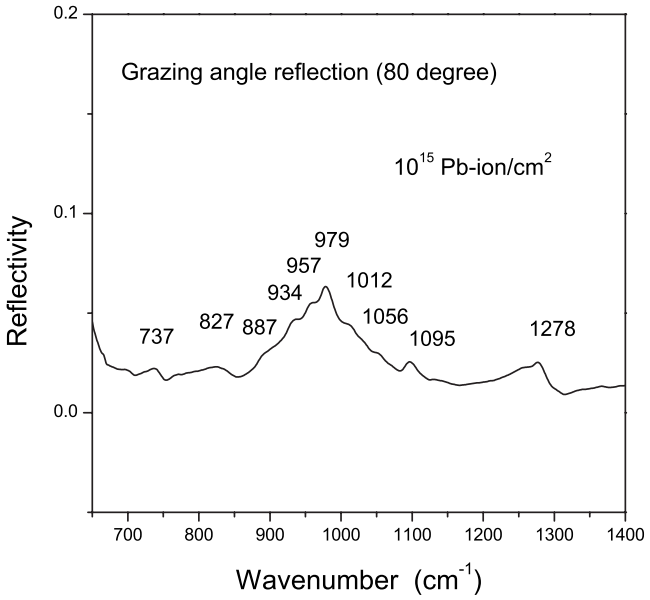

FIG. 2. Grazing angle IR reflectance spectrum (recorded with an 80° grazing angle objective) of Pb^+-irradiated zircon irradiated at 1×10^{15} Pb^+ ions/cm^2.

to vibrations related to ZrO_2, as was previously revealed in high-energy laser-treated zircon.[86] The broad feature between 1200 and 1300 cm^{-1}, in fact, contains two local maxima near 1240 and 1275 cm^{-1}, respectively. The features are due to vibration modes from the amorphous SiO_2.[86–88] The 1275 cm^{-1} band is attributed to a longitudinal optic (LO) mode of Si-O stretching,[87] and it is understood that the frequency can be affected by the way in which the amorphous state is produced. We note that the feature occurs as a very weak band near 1280 cm^{-1}, as indicated by an arrow in Fig. 1, in the crystal irradiated at 1×10^{14} Pb ions/cm^2, and it is undetectable in the crystal irradiated at a lower dose, i.e., 1×10^{13} Pb^+ ions/cm^2. A feature between 750 and 850 cm^{-1} forms at irradiation fluences as low as 1×10^{13} Pb^+ ions/cm^2, and its pattern becomes broad at 1×10^{15} Pb^+ ions/cm^2. It was a challenge to identify all of the phases and to completely assign all other Pb^+-irradiation-induced IR bands. How to best assign these complex bands is also arguable. Comparing the observational IR bands, as well as Raman bands (discussed in a later section), of the irradiated samples with the characteristic bands of synthetic lead silicates[89] suggests the presence of lead silicates in the irradiated samples. The results are evidenced by the occurrence of IR peaks near 827, 887, 934, 957, and 1056 cm^{-1} (Fig. 2), which are consistent with the five characteristic IR bands of $Pb_5Si_3O_{11}$ (at 840, 878, 934, and 1058 cm^{-1}) or $Pb_3Si_2O_7$ (at 845, 885, 938, 963, and 1062 cm^{-1}) reported by Furukawa *et al.*[89] This interpretation is further supported by the observation of the characteristic IR band near 127 cm^{-1} of lead silicates in polarized IR reflectance measurements.[80] The micro-infrared data seem to show that the lead silicate phases are more likely to be crystalline, whereas the overall pattern of the polarized IR spectra[80] of the Pb^+-irradiated samples is similar to those of disordered or defective lead silicates with high Pb contents (with Pb of 50–60 mol % in terms of PbO). However, considering the difference between the beam size used in the polarized IR (~3 mm) and this micro-infrared (~20 μm) measurements, the polarized IR measurements[80] are expected to give a "more-averaged" outcome, which suggests that both crystalline and amorphous lead silicates probably coexist in the Pb^+-irradiated samples. We also note that the damaged layers do not always show identical IR spectra when measuring the damaged layers with a beam diameter of 20 μm. The spectral variations associated with different areas are shown in Fig. 1, where three spectra sampled from three spots of the crystal irradiated at 1×10^{15} Pb^+ ions/cm^2 are also given.

Reflectance spectra from small thin pieces (200–500 μm in size) from the polycrystalline ceramic zircon irradiated with 10 MeV Au^{4+} ions at 1×10^{15} ions/cm^2 were recorded to further verify whether the irradiation can produce an amorphous phase(s) identical to those of metamict zircon and also to verify whether irradiation-induced decomposition of zircon into ZrO_2 and SiO_2 is the result at the highest fluences.[59] The effect of the Au^{4+} irradiation is evident in the IR reflectance spectrum (Fig. 3). The irradiation leads to a similar decease in reflectivity and a loss of detailed spectral features as seen in metamict zircon. The spectrum exhibits a broad feature between 700 and 1200 cm^{-1}, which is due to

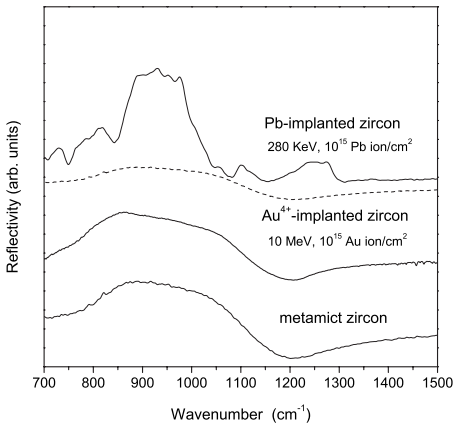

FIG. 3. Comparison of IR reflectance spectra of Pb^+- and Au^{4+}-irradiated zircon with that of natural metamict zircon (with f of ~1.0), whose crystal structure is damaged and amorphized by natural alpha-decay event processes over geological time. The dashed line indicates the feature of the aperiodic phase or domains of metamict zircon, which could coexist in the Pb^+-irradiated samples.

Si-O stretching bands associated with SiO_4 units.[81] Most importantly, the Au^{4+}-irradiated zircon exhibits an IR spectrum in the Si-O stretching region, which is essentially identical to that of metamict zircon. The results show that Au^{4+}-irradiated zircon contains the same amorphous phase as that found in metamict zircon, which is produced by alpha-decay event processes. The lack of spectral features of glassy SiO_2 between 1200 and 1300 cm^{-1} indicates that the irradiation did not cause the decomposition of zircon into SiO_2 and ZrO_2.

B. Raman spectra of Pb- and Au-irradiated zircon

All of the 12 predicted Raman modes ($2A_{1g}+4B_{1g}+B_{2g}+5E_g$) were observed in undamaged synthetic zircon (Fig. 4). They are the internal modes of SiO_4 groups: 1008 cm^{-1} (B_{1g}, ν_3, antisymmetric stretching), 975 cm^{-1} (A_{1g}, ν_1, symmetric stretching), 439 cm^{-1} (A_{1g}, ν_2, symmetric bending), 266 cm^{-1} (B_{2g}, ν_2, symmetric bending), and external modes:

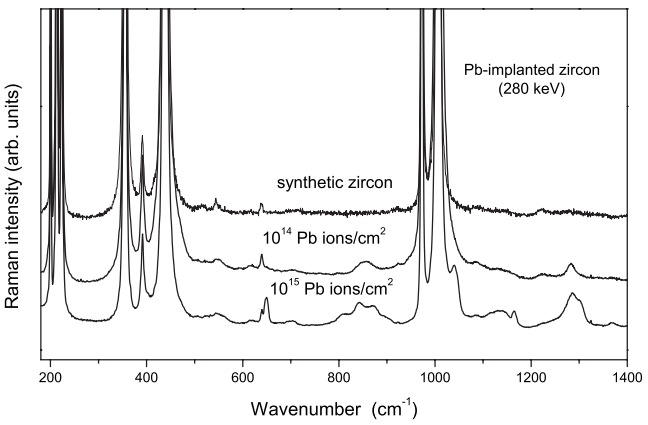

FIG. 4. Effect of Pb^+ irradiation on the Raman spectrum of zircon.

393, 355, 225, 214, and 202 cm^{-1}.[29,84,90–92] Our measurements also revealed weak bands in zircon at 545, 641, and 923 cm^{-1}. The 923 cm^{-1} mode is assigned as the ν_3 antisymmetric stretching due to its high frequency, whereas the 545 and 641 cm^{-1} bands are the two predicted antisymmetric bending modes (ν_4).

Irradiation of synthetic zircon with 280 keV Pb^+ ions at a fluence of 1×10^{13} Pb^+ ions/cm^2 leads to a decrease in the intensity of the Raman bands of zircon (a similar change has been seen in metamict zircon, e.g., Ref. 29), but it does not seem to result in significant or detectable changes in the spectral pattern nor does it produce amorphous phases sufficient to be detected, as its Raman spectrum shows features similar to those of the untreated sample and no extra signals are detected. The irradiation does not seem to have caused any significant change in frequencies and bandwidths (i.e., full width at half maximum (FWHM)) of Raman bands of zircon, especially for the ν_3 Raman band (B_{1g}, antisymmetric stretching), which exhibits significant changes in metamict zircon (discussed in a later section). In fact, the unirradiated crystal and those irradiated at 1×10^{13}, 1×10^{14}, and 1×10^{15} Pb^+ ions/cm^2 all show a band frequency near 1008 cm^{-1} and a FWHM of 2.2–3 cm^{-1}. The effect of irradiation with 280 keV Pb^+ ions at the high doses on the crystal structure of synthetic zircon is shown in Fig. 4. Samples irradiated with fluences of 1×10^{14} and 1×10^{15} Pb^+ ions/cm^2 exhibit not only a decrease in the intensities of the Raman bands of zircon, but also the presence of additional features (Fig. 4). Different laser excitations (488, 514, 568, and 632 nm) were also used to check if the additional signals are connected to laser-induced fluorescence, especially for the bands above 1200 cm^{-1}, since $ZrSiO_4$ and related compounds do not commonly show Raman bands in this region. The results indicate that the recorded additional features are due to Raman scattering rather than laser-induced fluorescence. The large number of irradiation-induced additional Raman bands indicates that the irradiation may have produced more than one phase. The presence of bands near 537, 565, and 749 cm^{-1} (Fig. 5), together with the bands near 1042 and 648 cm^{-1}, is indicative of the formation of nanograins of ZrO_2. A Raman band near 1040 cm^{-1} has been found in nanosized ZrO_2, and it is attributed to the surface mode of the nanomaterial.[93,94] The frequency and intensity are found to increase with deceasing grain size. Using the results for nanosized ZrO_2 and the peak position of the 1040 cm^{-1} band reported in Ref. 93, the ZrO_2 grains in the Pb^+-irradiated zircon are estimated to be as small as ~10 nm. The detection of a band near 648 cm^{-1} in the crystal irradiated at 1×10^{15} Pb^+ ions/cm^2 appears to indicate that tetragonal ZrO_2 might have formed, since the band position is in good agreement with that of a strong band for tetragonal ZrO_2 (Fig. 5). However, its strongest band located at 280 cm^{-1} was not detected. The Raman data show no evidence of the presence of cubic ZrO_2 [which, according to Ref. 95, has only one strong characteristic Raman band (F_{2g}) near 607 cm^{-1}] in any of the irradiated samples. The formation of ZrO_2 in zircon is expected to be accompanied by SiO_2, because of the decomposition of $ZrSiO_4$. Previous studies have suggested that decomposition-induced SiO_2 in radiation-damaged zircon is in the form of glasses (e.g.,

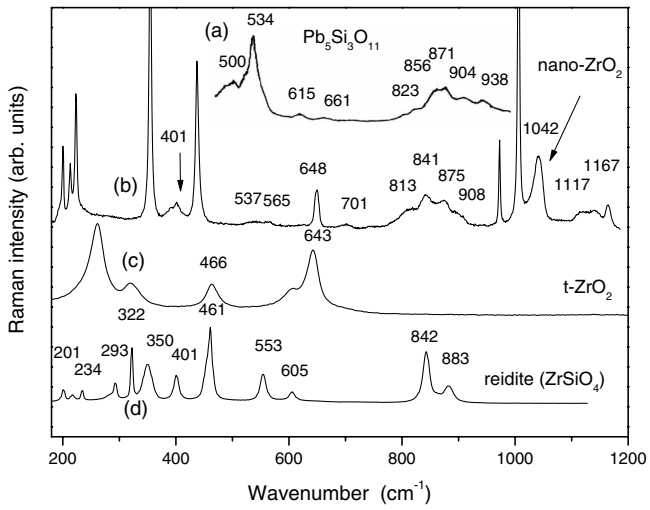

FIG. 5. Lead silicates are found in Pb^+-irradiated zircon (at 1×10^{15} Pb^+ ions/cm^2). (a) Raman spectrum of lead silicate (modified from Ref. 89). (b) Raman spectrum of Pb^+-irradiated zircon (bands with given frequencies are all extra features). (c) Spectrum of tetragonal zirconium oxide (t-ZrO_2). (d) Raman spectrum of reidite (high-pressure polymorph of zircon with a scheelite-type structure).

Refs. 25, 59, and 85), and this is supported by our IR data (Fig. 1). Bulk glassy SiO_2 commonly has weak Raman scattering and its strongest Raman band is located near 480 cm^{-1}. However, the Raman spectra of the irradiated zircon do not show these features. This is probably due to the relatively weak Raman intensity of glassy SiO_2, as compared to those of nanograined or crystalline ZrO_2, a phenomenon which has been previously noted in decomposed zircon.[96] The presence of glassy SiO_2 is probably evidenced by the broad bands between 1200 and 1300 cm^{-1}, which are due to LO bands of glassy SiO_2 and are also seen in the IR spectra (Fig. 1). The nanosize or stresses in the SiO_2 grains in the irradiated samples might lead to this LO feature being more easily detected. Several bands are located between 800 and 900 cm^{-1} in the crystal irradiated at 1×10^{15} Pb^+ ions/cm^2. The assignments of the Raman bands between 800 and 900 cm^{-1} and the identification of the related phases were not straightforward at the initial stage of the Raman and IR analyses, because previous spectroscopic studies[86] on decomposed zircon have not shown these bands, and also because most commonly known Zr- or/and Pb-related silicate minerals do not have similar Raman and IR features. It was tempting to interpret these bands as vibrations of reidite, a high-pressure polymorph of $ZrSiO_4$ with the scheelite-type structure ($I4_1/a$),[97,98] which has Si-O stretching bands at 842 and 883 cm^{-1} (as shown in Fig. 5 and Ref. 99). Reidite, which was recently found to exist as a natural mineral,[83] has also been observed in the irradiation of pressurized zircon with ^{238}U (the kinetic ion energy of ^{238}U is about 13.8 GeV) at a fluence of 2×10^9 U ions/cm^2 by Glasmacher *et al.*[100] However, a careful data analysis and further investigations suggest that the high-pressure phase of $ZrSiO_4$ should not be responsible for these additional bands in this Pb-irradiated zircon, because some intense Raman bands of reidite are

missing (Fig. 5) and also because zircon is reported to transform into reidite at pressures as high as 23 GPa in natural zircon,[97] or ~20 GPa in synthetic zircon.[101] The results of Glasmacher *et al.*[100] have shown that reidite can appear at a lower pressure (14.2 GPa) when high-energy ion irradiation is introduced, implying that the high-energy heavy-ion irradiation can generate an "effective" pressure effect (equivalent to a few GPa for their case). In fact, similar spectral changes for the ν_3 Raman band occur in experimentally shocked zircon and metamict zircon (see a later section). As compared with the ^{238}U implantation (kinetic ion energy of ~13.8 GeV),[100] the Pb^+ irradiations in this study were completed with a much lower ion energy (280 keV), at room temperature and under unpressurized conditions. The possible irradiation-produced pressure effect in these experiments, as well as in the natural metamictization process, is not expected to produce reidite domains. There, in fact, has been no evidence showing the presence of reidite in metamict zircon. However, we found that the peak positions (813, 841, 875, and 908 cm^{-1}) and the shape of these features between 800 and 900 cm^{-1} (Fig. 5) are consistent with laboratory-synthesized lead silicates.[89] The Raman results indicate that the formed lead silicates have a composition close to synthetic $Pb_5Si_3O_{11}$ or $Pb_3Si_2O_7$ ($Pb_5Si_3O_{11}$ has Raman bands at 823, 856, 871, 904, and 938 cm^{-1}, and $Pb_3Si_2O_7$ shows bands at 826, 857, 873, 908, and 937 cm^{-1}), although other phases are also expected to coexist because there are still several bands unassigned. This conclusion is further supported by the observation of weak, but well-resolved, IR bands peaked near 827, 887, 934, 957, and 1056 cm^{-1} (Figs. 1 and 2), which agree well with the characteristic IR bands of $Pb_5Si_3O_{11}$ or $Pb_3Si_2O_7$ in terms of frequency and number of bands (see earlier IR sections).

The Pb-irradiated crystal exhibits additional weak Raman bands near 65 and 120 cm^{-1} and a sharp feature near 82 cm^{-1} (Fig. 6), although they are not always present in every measured area. Those bands are not due to Raman bands of zircon and they are absent in untreated samples. The origins of these bands remain unclear. The data analysis shows that these bands are not due to $Pb_5Si_3O_{11}$ or $Pb_3Si_2O_7$, because their strong bands should be located near 100 or 157 cm^{-1}.[89] Alamosite ($PbSiO_3$ or $Pb_{12}Si_{12}O_{36}$ with a monoclinic structure, point group $2/m$) is a common natural lead silicate that occurs generally as a secondary mineral in the oxidized zone of lead-bearing base metal deposits. It has a large number of Raman bands between 100 and 1000 cm^{-1}, but was not identified in the irradiated samples. In order to further identify the Pb-containing phases or other phases that are responsible for these low-wave-number Raman bands, pure PbO, PbO_2 (with Pb^{4+}), Pb_3O_4 (with Pb^{2+} and Pb^{4+}), and $PbZrO_3$ were measured (Fig. 6). These Pb-related materials commonly show strong bands (mostly due to Pb-O stretching bands) below 200 cm^{-1}, but the identification of Raman features of PbO_2 in the irradiated zircon was not straightforward, because PbO_2 gives a weak Raman intensity and its Raman spectrum is very sensitive to experimental conditions.[102] These measured Pb-related materials (excluding lead silicates) are not expected to be associated with the irradiation-induced additional Raman features above 700 cm^{-1}, because they do not have fundamental vibrational

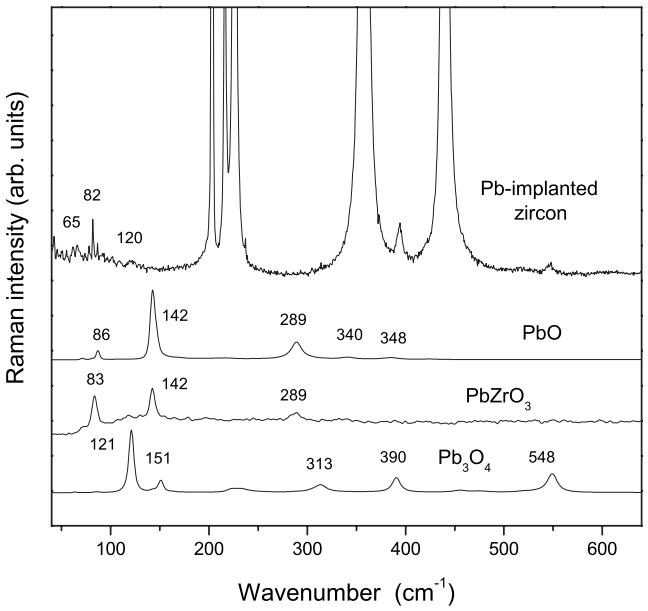

FIG. 6. Comparison of Raman spectrum of Pb-irradiated zircon with those of PbO, $PbZrO_3$, and Pb_3O_4.

bands in the region. Although the data suggest that PbO is not responsible for the low-wave-number Raman bands seen in Pb-irradiated zircon, the results are inconclusive and are incapable of completely ruling out the presence of Pb_3O_4, PbO_2, and $PbZrO_3$, because they all have at less one band with a frequency matching the 120 or the 82 cm^{-1} band in the irradiated zircon (Fig. 6). If any of these phases exists in the Pb^+-irradiated sample, they should be in limited amounts or at a trace level.

Similar to micro-infrared observations, the micro-Raman features and their intensity of irradiated zircon (1×10^{15} Pb^+ ions/cm^2) also vary with the sampled areas. A micro-Raman mapping analysis was carried out to estimate the degree of the heterogeneities of the Pb^+-irradiated surfaces. The results show systematic variations of the intensity of Raman bands attributed to zircon and irradiation-induced phases on a scale from a few to 10 μm, indicating that the local structure of the irradiated surface is heterogeneous.

The Raman measurements of Au-irradiated zircon (10 MeV Au^{4+} at 1×10^{15} Au^{4+} ions/cm^2) reveal that the most intense Raman-active ν_3 mode (B_{1g}) of zircon appears as a very weak feature near 1008 cm^{-1} over a background. This band can only be detected in limited areas under the Raman beam size of 1–2 μm even with different laser excitations, indicating that the sample is highly amorphized. The Raman feature is from limited residual grains of crystalline zircon heterogeneously distributed in the amorphous material or on the surface. The finding suggests that the irradiation with 10 MeV Au^{4+} ions at 1×10^{15} ions/cm^2 produces a more complete and homogeneous amorphization as well as a thicker amorphized layer, in comparison to the Pb^+-irradiated samples. The observation further confirms the results of the IR data (Fig. 3), which show that the sample is highly amorphized and exhibits a broad feature with a very low reflectivity. In contrast to the observation of the weak ν_3 mode of zircon, the conventional micro-Raman analysis on the amor-

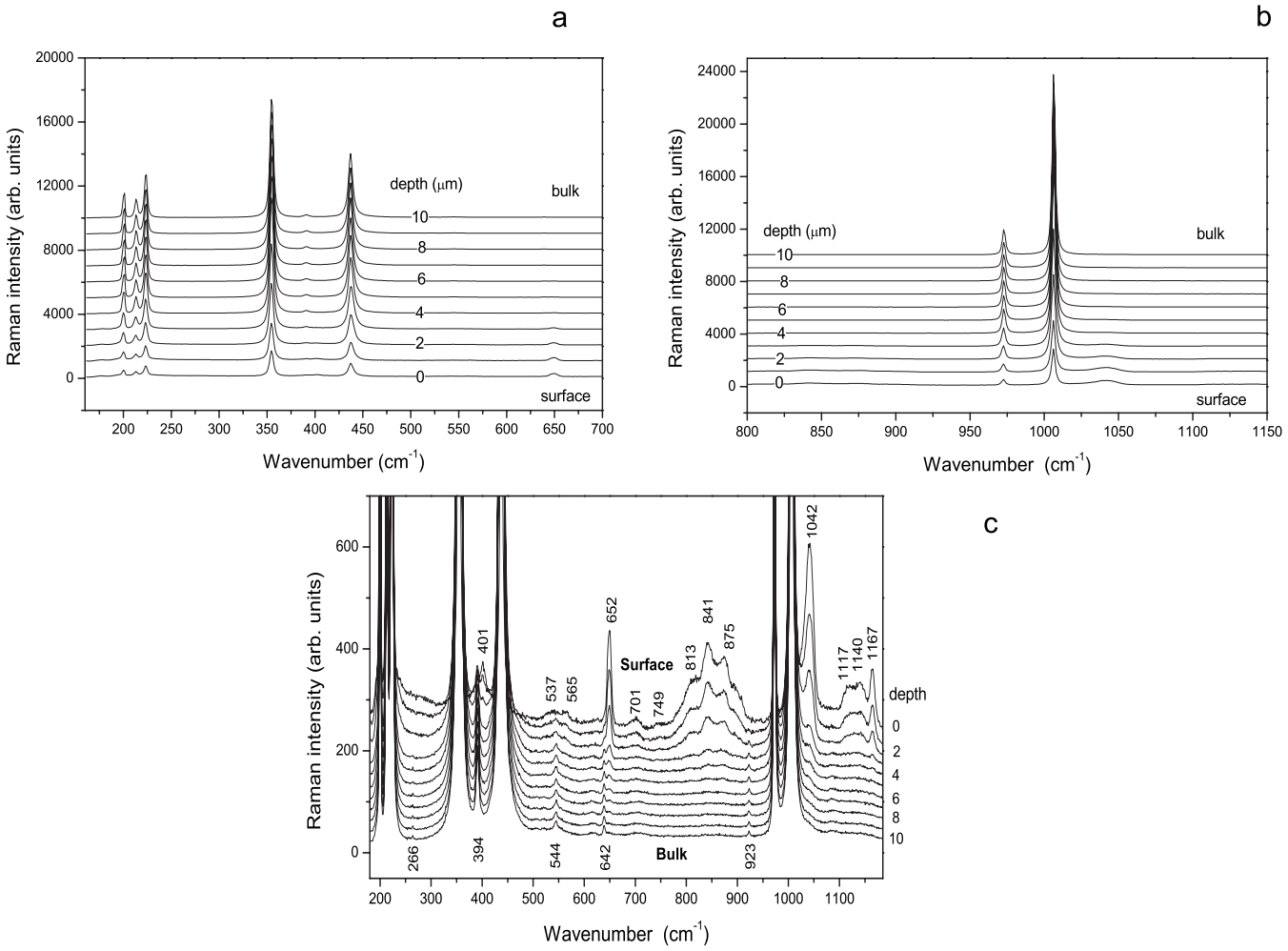

FIG. 7. Raman measurements with depth changes from the Pb-irradiated surface to the bulk of a zircon crystal: (a) data between 160 and 700 cm^{-1}, (b) between 800 and 1150 cm^{-1}, and (c) detailed spectra showing the change in the irradiation-induced additional bands. Note that for clarity, the top spectrum in (c) corresponds to that measured on the surface, whereas in (a) and (b), the spectra recorded on the surface are shown at the bottom. In (c), the band positions given above the spectrum recorded at the surface represent those of irradiation-induced additional features, and those appearing below those spectra measured in the bulk correspond to the band position of zircon.

phized phases in the Au^{4+}-irradiated ceramic zircon proved to be difficult even with different laser excitations. This is due to the fact that the measurements encountered a strong background that is likely to result from irradiation-induced color centers in the sample (the irradiation caused the milky ceramic zircon to become black). Even the use of FT-Raman, whose laser excitation is in the near infrared region and which is commonly ideal for dealing with laser fluorescence, did not help to overcome this difficulty. The problem is also believed to be partly caused by the very low scattering of the radiation-induced amorphous phase, since Raman measurements[29] have shown that the Raman scattering intensity of highly metamict zircon and the amorphous phase is more than ten times lower than that of undamaged zircon. This difficulty was previously encountered by some Raman studies of metamict zircon, which did not succeed in detecting the signals of the amorphous phase. Comparing the Raman and IR data of Au^{4+}-irradiated zircon suggests that the IR technique is a better and more sensitive tool for characterizing the amorphous phase in zircon.

C. Results from depth-dependent measurements

The depth dependence of the Raman spectra was investigated for zircon irradiated with Pb^+ at fluences of 1×10^{15} Pb^+ ions/cm^2 [Figs. 7(a)–7(c)]. These measurements are based on the confocal mechanism of the Raman spectrometry. Figures 7(a)–7(c) show the variation of Raman spectra recorded from the surface to the bulk. The irradiation-induced features are more clearly shown in Fig. 7(c). The changes occur in three aspects. First, in spite of the fact that more undamaged zircon is expected to be recorded inside the bulk than close to the surface, it seems significant that the intensity of the Raman bands of zircon shows a systematic increase from the damaged surface to the undamaged bulk [Figs. 7(a), 7(b), and 8(a)]. Second, variations of spectral features are detected and their intensity decreases when the sampling spots change from the surface to the bulk [Figs. 7(c) and 8(a)]. This finding further indicates that the extra signals are from the surface layer and are due to the Pb^+ irradiation. Third, the peak profiles (band frequency and

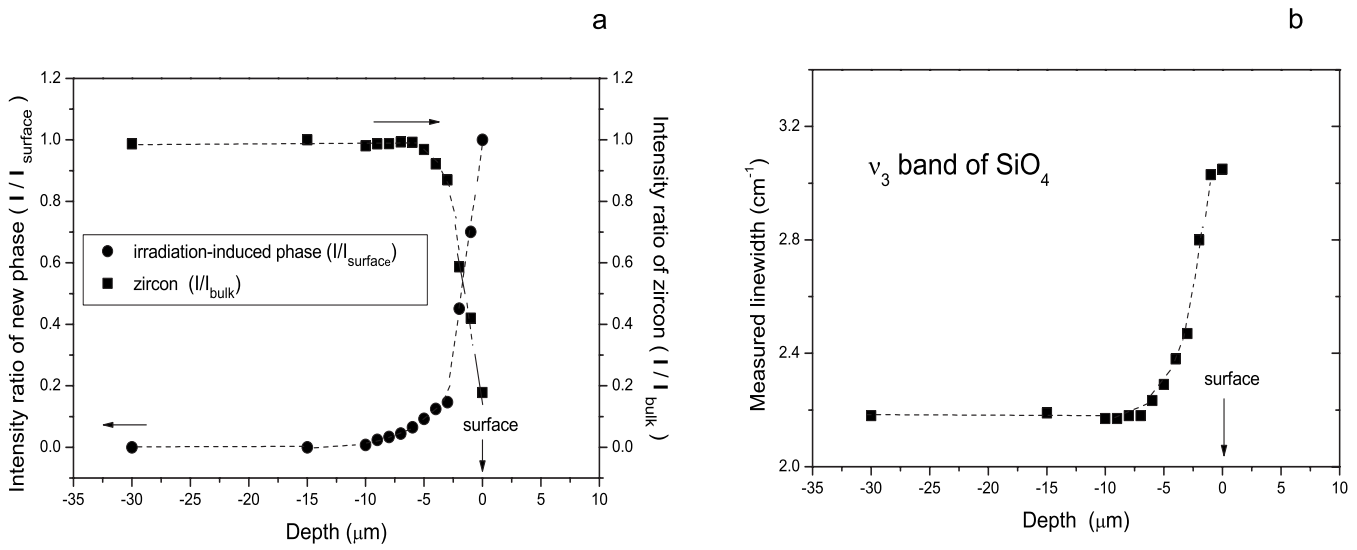

FIG. 8. Raman band profiles from the damaged surface to the bulk of irradiated zircon (at 1×10^{15} Pb^{+} ions/cm^2): (a) depth dependence of reduced Raman intensities for the ν_3 band of zircon and the irradiation-induced band near 841 cm^{-1}; (b) depth dependence of the measured bandwidth (full width at half maximum) of the ν_3 mode (near 1008 cm^{-1}) of zircon. The dramatic changes near the surface are due to Pb^{+}-irradiation damage.

FWHM) of the Raman bands of zircon show no or little change while varying the depth [Figs. 8(a) and 8(b)]. For example, the frequency of the ν_3 Raman band near 1008 cm^{-1} is nearly depth independent. The FWHM of the ν_3 band gives a measured value of ~3.0 cm^{-1} on the surface, and it drops to 2.3 cm^{-1} at a depth of 5 μm. The parameter has almost a constant value (2.2 cm^{-1}) at a depth of 10–30 μm [Fig. 8(b)]. The depth dependence indicates that the impact of irradiation can occur in the depth of a few micrometers in terms of Raman spectroscopy, although the amorphized layer is expected to be as thin as tens and hundreds of nanometers.[54,63] The findings from depth-dependent measurements further confirm the observation (see an earlier section) that the irradiation causes little change in the frequency and width of the Raman bands of zircon, in sharp contrast to those from matamict zircon and zircon treated by other processes, such as laser irradiation and high-pressure shock [Figs. 9(a)–9(d)].

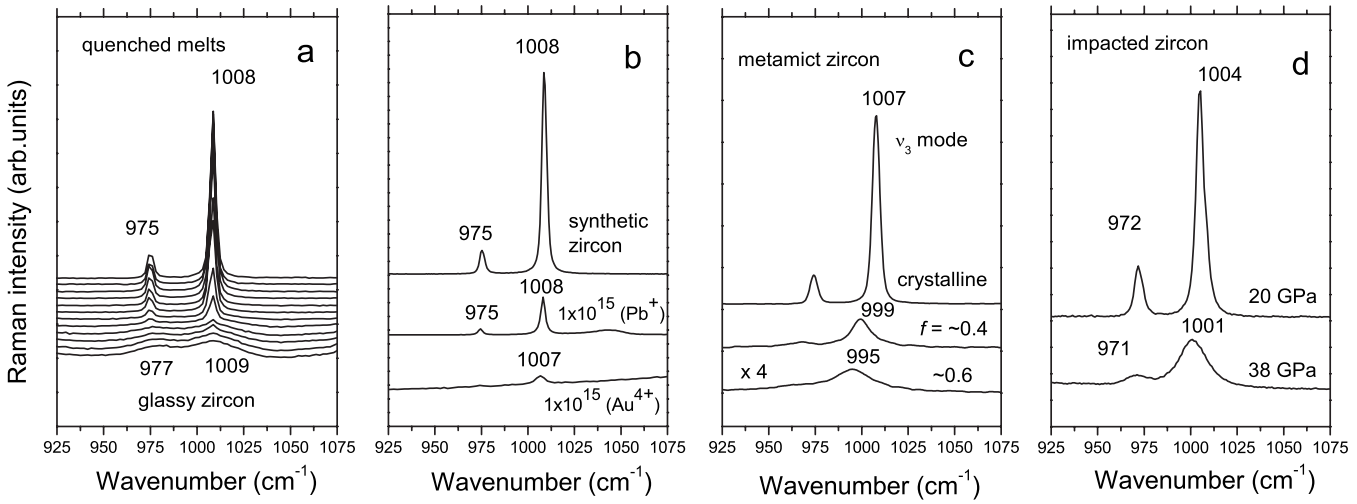

FIG. 9. The effect of different physical processes on the frequency and width of the ν_3 Raman mode of zircon: (a) laser irradiation and melting [modified from Ref. 86; the spectra are recorded along a length of 12 μm crossing the boundary between the unmolten (with sharp features) and molten (with broad features) regions]; (b) 280 keV Pb^{+} and 10 MeV Au^{4+} irradiations; (c) natural metamictization (f is the fraction of amorphous phase in natural zircon produced by metamictization); and (d) high-pressure shocking (with shocking pressures of 20 and 38 GPa). The data show that different physical processes may result in different changes in the phonon modes of zircon. Quenched "glass" $ZrSiO_4$ from high-temperature melting shows that the ν_3 Raman mode shifts to a higher frequency and becomes broad significantly, while the ion irradiations lead to no or little change in frequency and bandwidth. In contrast to (a) and (b), metamictization and high-pressure shocking both cause a significant decrease in the band frequency and a band broadening.

IV. DISCUSSION

A. Amorphous states of zircon caused by different irradiation techniques

One of the key issues concerning the different approaches in the study of metamictization and amorphization in zircon is to clarify whether or not the different experimental approaches result in consistent observations and, if not, how to evaluate and explain the possibly different outcomes for each irradiation method. Previous studies[96] have led to unanswered questions and concerns, e.g., what is the relationship between the structural characteristics of disordered materials and the type of irradiation or physical process used to produce them?

Early studies on metamictization generally considered the metamict minerals as "glasslike" materials, and referred to the metamict state as a glassy state similar to that produced by rapid quenching of melts. However, experimental evidences have emerged that suggest that there are important differences between the aperiodic states depending on whether they result from a quenched melt or from irradiation. Structural differences between the glass state obtained by thermally quenching melts and ion-beam-amorphized states have been reported for lead pyrophosphate.[103] IR studies[79] on the structures of metamict titanite ($CaTiSiO_5$) and its glass analog (with the same chemical composition) produced by quenching melts have shown that the two types of materials have different vibrational features (especially in the Ti-O and Si-O stretching regions), although they are both amorphous in terms of transmission electron microscopy or x-ray diffraction analysis. An extended x-ray-absorption fine structure study[104] of the Zr, Th, and U sites in aperiodic and/or metamict $(Ca,Th)ZrTi_2O_7$ (zirconolite) has suggested that there are fundamental structural differences in cation environments between radiation-induced aperiodic (metamict) phases and glasses quenched from melts. Zircon has a high melting temperature (above 2700–2800 K), and crystalline ZrO_2 and a liquid of SiO_2 coexist for a composition of $ZrSiO_4$ between ~1960 and ~2670 K.[105] Although it is difficult to quench zircon melts without decomposition into ZrO_2 and SiO_2, glasslike zircon ($ZrSiO_4$) has been found near the boundaries between the molten and unmolten regions (where a large temperature gradient occurs).[86] The large temperature gradient is likely to enhance the quench rate and facilitate a "freeze" of the local configuration of the zircon melts before the decomposition takes place. The effects of high-temperature melting, ion irradiations, metamictization, and high-pressure shocking on zircon are compared in Figs. 9(a)–9(d). These experimental results indicate that the metamict state is different from the glassy state obtained by quenching. The results from Pb- and Au-irradiated zircon further confirm that the ballistic effects of the recoil nucleus of the alpha-decay process are different from that occurring in high-temperature melting processes. Apparently, the processes and structural states associated with metamictization and irradiation amorphization are more complex than those in common glasses. The formation of the metamict state involves not only amorphization, but also defect accumulation caused by alpha-particle damage (see a later section) and further radiation or irradiation may lead to damage as well as recrystallization. The IR spectrum of Au^{4+}-irradiated zircon shows a broad Si-O stretching feature extending between 800 and 1200 cm^{-1}, indicating that short-range order remains in the amorphized phases, and Si and O atoms form SiO_4 tetrahedra that have additional linkages different from the one in crystalline zircon. There were, in fact, no clear experimental evidences to confirm or rule out whether heavy-ion-beam amorphization, as a technique to simulate the impact of recoils in alpha-decay processes, can really produce the same amorphous phases seen in metamict zircon. The results from the present experimental investigation, especially the data from Au^{4+}-irradiated zircon, show that high-energy heavy-ion irradiations can, in fact, produce an amorphous phase that is similar to that observed in natural metamictization processes, although the very high dose implantation of ions might, in some circumstances, lead to the formation of additional phases during the process.

B. Formation of additional phases and decomposition of Pb-irradiated zircon

Additional phases and clusters or domains are observed in the Pb-irradiated zircon, in contrast to metamict and Au-irradiated zircon. Their occurrence raises interesting questions, such as how and why they formed. SiO_2 and ZrO_2 have been previously reported during ion irradiation of zircon[59] at high temperatures, in heated metamict zircon,[13,23,25,85,96] in heated Pu-doped zircon,[44] and in quenched zircon melts.[86] Most of the observations of ZrO_2 in zircon involved heating the damaged samples to high temperatures. One may speculate that the decomposition occurring in the Pb^+-irradiated zircon is caused by ion beam heating of the already amorphized phases during further irradiation. The very different spectral patterns and the different final phases seen in the Pb^+-irradiated zircon and those of thermally treated zircon by furnace heating or laser melting indicate that the decomposition occurring in the Pb^+-irradiated zircon is associated with processes different from those zircon treated at high temperatures, i.e., it is not mainly due to high-temperature decomposition. The close proximity of the damage production peak to the surface (35 nm) may enhance decomposition and formation of additional phases, since the surface can promote segregation under these conditions. The high sputtering probability may also result in some surface nonstoichiometry. The formation of additional phases and decomposition of $ZrSiO_4$ in Pb-irradiated sample may also be due to the Pb ion itself; however, the Au^{4+} irradiation (for which Au ions are chemically inert and are not expected to easily form phases with Si or Zr) does not cause similar changes. Although zircon is widely used for U/Pb age dating in geology, Pb concentrations in natural zircon are generally at trace element levels (tens of ppb to hundreds of ppm).[106] High-Pb-content zircon is rare, although zircon can easily accommodate other elements. Experiments and synthesis have indicated that zircon tends to reject the incorporation of Pb, resulting in the occurrence of alamosite (a phase of lead silicate, $PbSiO_3$).[106] In addition, metal Pb nanoparticles have recently been seen in

both Pb^+-irradiated and natural zircon.[40,63] The observation of lead silicates in the present study further indicates the degree to which the crystal structure of zircon resists the incorporation of high contents of Pb. It is likely that during the irradiation processes, some of the highly concentrated Pb ions, instead of finding their way into the structural sites in zircon through replacing Zr and forming $Zr_xPb_{1-x}SiO_4$, initially accumulate locally to a degree that rarely occurs in natural zircon. They might react with other elements (e.g., oxygen) and form some kind of Pb-O bonds (or local clusters) that finally lead to the appearance of lead silicates with further Pb irradiation and increasing Pb contents. In contrast to Pb ions, Au ions are especially chemically inactive, so they are less likely to react with other elements to form Au-related phases. It is reported that lead silicates can form at temperatures below 673 K,[89] indicating relatively low activation energies. Lead silicates have complex structures in which PbO_4 and PbO_3 pyramids, SiO_4, SiO_3, and Si_2O_7 can be basic structural units depending on their chemical compositions and structures.[89,107] The formation of the phases or the occurrence of the bonding between O and Pb may modify the local charge balance, cation coordination, and local chemical compositions. These variations are likely to occur simultaneously or eventually cause the appearance of ZrO_2 and SiO_2 as a result of irradiation and local decomposition.

C. Effect of ion irradiation on vibrational band frequencies of zircon and defective structure of zircon domains

One of the important and interesting observations from the present study is the limited impact of Pb^+ and Au^{4+} irradiations on the frequency and FWHM of the vibrational modes of zircon. An earlier Raman study[26] has reported that the ν_3 Raman band near 1008 cm^{-1} can shift down to ~955 cm^{-1} and become broad in metamict zircon samples. Further detailed studies have focused on the change in band frequency and FWHM as a function of the degree of the radiation damage.[29,32,37,108–111] These later studies have shown that for metamict zircon, the FWHM of the 1008 cm^{-1} band can become as large as ~30 cm^{-1} (an increase by more than 900%) in partially metamict zircon. This Raman band and its changes have been used to estimate or determine the degree of radiation damage in natural zircon and even to study or identify other natural events or incidents that natural crystals from some geological locations might have experienced. However, the same Raman band shows no or little change in peak positions and FWHM in both Pb- and Au-irradiated zircon [the irradiation-induced frequency change for this antisymmetric stretching band (ν_3) of SiO_4 is less than 1 cm^{-1} in the samples with fluences up to 1×10^{15} Pb^+ ions/cm^2 and 1×10^{15} Au^{4+} ions/cm^2; and the change is not significant because our instrumental resolution is around 2 cm^{-1}], although a dramatic decrease in its band intensity occurs and similar amorphous domains seen in metamict zircon form. The results suggest that the response of the phonon bands to the high-energy heavy-ion irradiation is different from their reaction to metamictization (i.e., vibrational modes of zircon behave differently in response to heavy-ion irradiation and metamictization). The observed different behaviors raise some interesting questions. What is the physics behind the frequency decrease and broadening in the ν_3 mode, as well as other vibrational bands of zircon, during metamictization? Why does it not occur during Pb^+ and Au^{4+} irradiations? To what extent are the band's frequency and FWHM correlated to radiation damage in the material? The frequency of a phonon mode gives the energy of the vibration (or the energy difference between the two transition levels), and it depends on the molecular structure and environment. Atomic mass, force constants, bond strength, bond order, molecular substituents, molecular geometry, and hydrogen bonding all may alter the vibrational force constant which, in turn, dictates the vibrational energy. In addition, the width of a Raman mode or a vibration mode, which is connected to the inverse of the phonon lifetime is an important parameter that is sensitive to structural variations. In solid-state materials, the frequency and width of phonon vibrations can be affected by various factors, such as temperature, pressure, isotopic compositions, inhomogeneity of compositions, different types of defects, structural disorders, defect concentrations, anharmonic coupling, stress inhomogeneity, grain size, and electron-phonon coupling.[112] For metamict zircon, the causes of the shift of the ν_3 band and its dramatic broadening in radiation-damaged zircon were proposed to be due to a defective crystal structure of the remaining crystalline grains or domains in metamict zircon (e.g., Refs. 29, 96, and 110). The ν_3 Raman band (near 1008 cm^{-1}) is due to characteristic vibrations of zircon, and it does not originate from amorphized domains. Investigations by vibrational spectroscopy have shown that the spectra of metamict minerals have contributions from both the amorphous phases and defective crystalline domains.[81,113] The change in band frequency and width corresponds to the reported metamictization-induced variations of the zircon crystal structure, such as the significant increase in its unit cell parameters (e.g., Refs. 11, 18, and 19) and the defected lattice,[114] which are responsible, together with the amorphous phase, for the volume swelling of metamict zircon. The defective nature related to the change in the band has been shown by Raman studies,[96,110] which indicate that annealing metamict zircon at temperatures of 500–700 K (the crystallization temperature for zircon is about 1000 K) for a period of time as small as a few seconds leads to a recovery of the band position and FWHM. Experimental evidence also shows that the peak profile of the band is affected not only by metamictization but also by other processes such as melting and pressure impact (Fig. 9). The implication of our observation, that the Raman band frequency and FWHM remain unchanged after the Pb and Au irradiations, is that these irradiations do not produce the same defective crystalline domains as the alpha-decay radiation or metamictization does in natural zircon. Ion-irradiation-induced frequency shifts and band broadening have been reported in some studies. However, as compared with the change (up to ~50 cm^{-1} for frequency, and up to ~30 cm^{-1} for FWHM) of the ν_3 Raman band in metamict zircon, the reported changes caused by ion beam irradiation are generally much smaller in magnitude (a few to 10 cm^{-1}).[115–119]

The different response of the vibrational mode to metamictization and high-energy Pb-ion and Au-ion irradiations is

expected to be due to the different processes involved in the two types of damage. The radiation damage process for an alpha-decay event is generally well understood (e.g., Ref. 4). The alpha particle dissipates most of its energy by ionization, and after undergoing enough elastic collisions along its path, it displaces several hundred atoms, thereby producing defects. The energy of the recoil nucleus, on the other hand, is lost primarily through elastic collisions with atoms in the structure, creating several thousand atomic displacements forming "tracks" of amorphous or disordered materials. However, the Pb-ion and Au-ion irradiations primarily involve only one process—the amorphization and damage related to the recoil, and there is a lack of the impacts and damage caused by alpha particles in metamictization. This may explain why the crystalline domains of zircon samples irradiated by high-energy Pb and Au ions show residual crystalline structures that are less defective than that seen in metamict zircon. It is clear that for studying and modeling the metamictization process, especially the radiation-induced defective crystal structure and its swelling and defect behavior, it is necessary to consider the impact of alpha-particle damage. It is also worth noting that although the alpha-particle radiation is expected to cause damage in the lattice of zircon, the Au-irradiated zircon (for which no alpha-particle damage was involved) has an amorphized phase similar to that of metamict zircon. This, in fact, confirms that it is the recoil process, rather than the alpha particle, that has a more critical and decisive role in the amorphization process and the final structure of the amorphized phase, and that the role played by the alpha particle in the final state or phases of the amorphization, in fact, appears to be limited.

V. CONCLUSIONS

In summary, this study demonstrates that sufficiently energetic heavy ions, which are inert, such as 10 MeV Au^{4+} ions, result in a completely amorphous state that is similar to that found in fully metamict natural zircons. In contrast, irradiation with low-energy heavy ions that are reactive, such as 280 keV Pb^{+} ions, can result in secondary phase formation. The study also shows that the spectral features of Au^{4+}- and Pb^{+}-irradiated zircon are different from those of quenched $ZrSiO_4$ melts. Finally, there remains some discrepancies between the structure of the damaged state in metamict zircon compared to the amorphous or damaged state in the 10 MeV Au^{4+} zircon, and this difference is attributed to the role of the alpha particle in natural minerals in producing defects in the residual crystalline domains that may remain.

ACKNOWLEDGMENTS

Financial funding from the British Nuclear Fuel Ltd. (BNFL) and the Cambridge-MIT Institute (CMI) is gratefully acknowledged. The research at ORNL was sponsored by the Division of Materials Sciences and Engineering, Office of Basic Energy Sciences, U.S. Department of Energy under Contract No. DE-AC05-00OR22725 with Oak Ridge National Laboratory, managed and operated by UT-Battelle, LLC. R.C.E. gratefully acknowledges financial support from the Office of Basic Energy Science, U.S. Department of Energy through Grant No. DE-FG02-97ER45656. W.J.W. and Y.Z. were supported by the Office of Basic Energy Sciences, U.S. Department of Energy under Contract No. DE-AC05-76RL01830.

*mz10001@esc.cam.ac.uk

[1] E. B. Anderson, B. E. Burakov, and V. G. Vasiliev, in Proceedings of the International Conference SAFE WASTE '93, Avignon, France, June 13–18, 1993, MRS Symposia Proceedings No. 2 (1993), pp. 29–33.
[2] R. C. Ewing, W. Lutze, and W. J. Weber, J. Mater. Res. **10**, 243 (1995).
[3] W. J. Weber, R. C. Ewing, and A. Meldrum, J. Nucl. Mater. **250**, 147 (1997).
[4] W. J. Weber, R. C. Ewing, C. R. A. Catlow, T. D. de la Rubia, L. W. Hobbs, C. Kinoshita, H. Matzke, A. T. Motta, M. Nastasi, E. K. H. Salje, E. R. Vance, and S. J. Zinkle, J. Mater. Res. **13**, 1434 (1998).
[5] R. C. Ewing, Proc. Natl. Acad. Sci. U.S.A. **96**, 3432 (1999).
[6] R. C. Ewing, Earth Planet. Sci. Lett. **229**, 165 (2005).
[7] R. C. Ewing, Nucl. Instrum. Methods Phys. Res. B **91**, 22 (1994).
[8] L. W. Hobbs, F. W. Clinard, Jr., S. J. Zinkle, and R. C. Ewing, J. Nucl. Mater. **216**, 291 (1994).
[9] R. C. Ewing, A. Meldrum, L. M. Wang, and S. X. Wang, Rev. Mineral. Geochem. **39**, 317 (2000).
[10] R. C. Ewing, A. Meldrum, L. M. Wang, W. J. Weber, and L. R. Corrales, Rev. Mineral. Geochem. **53**, 387 (2003).
[11] H. D. Holland and D. Gottfried, Acta Crystallogr. **8**, 291 (1955).
[12] P. J. Wasilewski, F. E. Senftle, J. E. Vaz, A. N. Thorpe, and C. C. Alexander, Radiat. Eff. **17**, 191 (1973).
[13] E. R. Vance, Radiat. Eff. **24**, 1 (1975).
[14] H. Özkan, J. Appl. Phys. **47**, 4772 (1976).
[15] R. L. Barinsky and I. M. Kulikova, Phys. Chem. Miner. **1**, 325 (1977).
[16] B. C. Chakoumakos, T. Murakami, G. R. Lumpkin, and R. C. Ewing, Science **236**, 1556 (1987).
[17] K. Yada, T. Tanji, and I. Sunagawa, Phys. Chem. Miner. **14**, 197 (1987).
[18] T. Murakami, B. C. Chakoumakos, R. C. Ewing, G. R. Lumpkin, and W. J. Weber, Am. Mineral. **76**, 1510 (1991).
[19] W. J. Weber, J. Mater. Res. **5**, 2687 (1990).
[20] J. A. Woodhead, G. R. Rossman, and L. T. Silver, Am. Mineral. **76**, 74 (1991).
[21] J. A. Woodhead, G. R. Rossman, and A. P. Thomas, Am. Mineral. **76**, 1533 (1991).
[22] Z. Mursic, T. Vogt, H. Boysen, and F. Frey, J. Appl. Crystallogr. **25**, 519 (1992).
[23] S. Ellsworth, A. Navrotsky, and R. C. Ewing, Phys. Chem. Miner. **21**, 140 (1994).
[24] F. Farges, Phys. Chem. Miner. **20**, 504 (1994).
[25] A. C. McLaren, J. D. Fitz, and I. S. Williams, Geochim. Cosmochim. Acta **58**, 993 (1994).

[26] L. Nasdala, G. Irmer, and D. Wolf, Eur. J. Mineral. **7**, 471 (1995).
[27] E. K. H. Salje, J. Chrosch, and R. C. Ewing, Am. Mineral. **84**, 1107 (1999).
[28] S. Ríos, E. K. H. Salje, M. Zhang, and R. C. Ewing, J. Phys.: Condens. Matter **12**, 2401 (2000).
[29] M. Zhang, E. K. H. Salje, I. Farnan, A. Graem-Barber, P. Danial, R. C. Ewing, A. M. Clark, and H. Leroux, J. Phys.: Condens. Matter **12**, 1915 (2000).
[30] G. C. Capitani, H. Leroux, J. C. Doukhan, S. Ríos, M. Zhang, and E. K. H. Salje, Phys. Chem. Miner. **27**, 545 (2000).
[31] I. Farnan and E. K. H. Salje, J. Appl. Phys. **89**, 2084 (2001).
[32] L. Nasdala, M. Wenzel, G. Vavra, G. Irmer, T. Wenzeland, and B. Kober, Contrib. Mineral. Petrol. **141**, 125 (2001).
[33] M. Zhang, E. K. H. Salje, and R. C. Ewing, J. Phys.: Condens. Matter **15**, 3445 (2003).
[34] T. Geisler, K. Trachenko, S. Ríos, M. T. Dove, and E. K. H. Salje, J. Phys.: Condens. Matter **15**, L597 (2003).
[35] T. Geisler, M. Zhang, and E. K. H. Salje, J. Nucl. Mater. **320**, 280 (2003).
[36] S. Ríos and T. Boffa-Ballaran, J. Appl. Crystallogr. **36**, 1006 (2003).
[37] C. S. Palenik, L. Nasdala, and R. C. Ewing, Am. Mineral. **88**, 770 (2003).
[38] I. Farnan, E. Balan, C. J. Pickard, and F. Mauri, Am. Mineral. **88**, 1663 (2003).
[39] S. E. Ashbrook and I. Farnan, Solid State Nucl. Magn. Reson. **26**, 105 (2004).
[40] S. Utsunomiya, C. S. Palenik, J. W. Valley, A. J. Cavosie, S. A. Wilde, and R. C. Ewing, Geochim. Cosmochim. Acta **68**, 4679 (2004).
[41] E. K. H. Salje, Appl. Phys. Lett. **89**, 131902 (2006).
[42] S. Utsunomiya, J. W. Valley, A. J. Cavosie, S. A. Wilde, and R. C. Ewing, Chem. Geol. **236**, 92 (2007).
[43] I. Farnan, H. Cho, and W. J. Weber, Nature (London) **445**, 190 (2007).
[44] W. J. Weber, Radiat. Eff. Defects Solids **115**, 341 (1991).
[45] W. J. Weber, J. Am. Ceram. Soc. **76**, 1729 (1993).
[46] W. J. Weber, R. C. Ewing, and L. M. Wang, J. Mater. Res. **9**, 688 (1994).
[47] N. J. Hess, W. J. Weber, and S. D. Conradson, J. Alloys Compd. **271**, 240 (1998).
[48] J. A. Fortner, Y. Badyal, D. C. Price, J. M. Hanchar, and W. J. Weber, in *Microstructural Processes in Irradiated Materials*, edited by S. J. Zinkle, G. Lucas, R. C. Ewing, and J. Williams, MRS Symposia Proceedings No. 540 (Materials Research Society, Warrendale, PA, 1999), pp. 349–354.
[49] B. D. Begg, N. J. Hess, W. J. Weber, S. D. Conradson, M. J. Schweiger, and R. C. Ewing, J. Nucl. Mater. **278**, 212 (2000).
[50] B. E. Burakov, E. B. Anderson, M. V. Zamoryanskaya, M. A. Yagovkina, E. E. Strykanova, and E. V. Nikolaeva, in *Scientific Basis for Nuclear Waste Management XXIV* (Symposium held August 27–31, 2000, Sydney, Australia), edited by K. P. Hart and G. R. Lumpkin, MRS Symposia Proceedings No. 663 (Materials Research Society, 2001), pp. 307–313.
[51] B. E. Burakov, J. M. Hanchar, M. V. Zamoryanskaya, V. N. Garbuzov, and V. A. Zirlin, Radiochim. Acta **89**, 1 (2002).
[52] L. A. Bursill and G. Braunshausen, Philos. Mag. A **62**, 395 (1990).
[53] L. Babsail, N. Hamelin, and P. D. Townsend, Nucl. Instrum. Methods Phys. Res. B **59**, 1219 (1991).
[54] D. J. Cherniak, W. A. Lanford, and F. J. Ryerson, Geochim. Cosmochim. Acta **55**, 1663 (1991).
[55] B. C. Chakoumakos, W. C. Oliver, G. R. Lumpkin, and R. C. Ewing, Radiat. Eff. Defects Solids **118**, 393 (1991).
[56] R. K. Eby, R. C. Ewing, and R. C. Birtcher, J. Mater. Res. **7**, 3080 (1992).
[57] L. M. Wang and R. C. Ewing, Nucl. Instrum. Methods Phys. Res. B **65**, 324 (1992).
[58] W. C. Oliver, J. C. McCallum, B. C. Chakoumakos, and L. A. Boatner, Radiat. Eff. Defects Solids **132**, 131 (1994).
[59] A. Meldrum, S. J. Zinkle, L. A. Boatner, and R. C. Ewing, Nature (London) **395**, 56 (1998).
[60] A. Meldrum, L. A. Boatner, W. J. Weber, and R. C. Ewing, Geochim. Cosmochim. Acta **62**, 2509 (1998).
[61] A. Meldrum, S. J. Zinkle, L. A. Boatner, and R. C. Ewing, Phys. Rev. B **59**, 3981 (1999).
[62] S. X. Wang, L. M. Wang, and R. C. Ewing, Phys. Rev. B **63**, 024105 (2000).
[63] J. Lian, S. Rios, L. A. Boatner, L. M. Wang, and R. C. Ewing, J. Appl. Phys. **94**, 5695 (2003).
[64] R. E. Williford, B. D. Begg, W. J. Weber, and N. J. Hess, J. Nucl. Mater. **278**, 207 (2000).
[65] R. E. Williford, W. J. Weber, R. Devanathan, and A. N. Cormack, J. Nucl. Mater. **273**, 164 (1999).
[66] K. Trachenko, M. T. Dove, and E. Salje, J. Appl. Phys. **87**, 7702 (2000).
[67] M. J. Akhtar and S. Waseem, Chem. Phys. **274**, 109 (2001).
[68] B. Park, W. J. Weber, and L. R. Corrales, Phys. Rev. B **64**, 174108 (2001).
[69] K. Trachenko, M. T. Dove, and E. K. H. Salje, Phys. Rev. B **65**, 180102(R) (2002).
[70] K. Trachenko, M. T. Dove, and E. K. H. Salje, J. Phys.: Condens. Matter **15**, L1 (2003).
[71] E. Balan, F. Mauri, C. J. Pickard, I. Farnan, and G. Calas, Am. Mineral. **88**, 1769 (2003).
[72] R. Devanathan, L. R. Corrales, W. J. Weber, A. Chartier, and C. Meis, Phys. Rev. B **69**, 064115 (2004).
[73] H. L. Heinisch and W. J. Weber, Nucl. Instrum. Methods Phys. Res. B **228**, 293 (2005).
[74] R. Devanathan, L. R. Corrales, W. J. Weber, A. Chartier, and C. Meis, Nucl. Instrum. Methods Phys. Res. B **228**, 299 (2005).
[75] J. M. Pruneda, L. Le Polles, I. Farnan, K. Trachenko, M. T. Dove, and E. Artacho, Mol. Simul. **31**, 349 (2005).
[76] J. M. Pruneda and E. Artacho, Phys. Rev. B **71**, 094113 (2005).
[77] R. Devanathan, L. R. Corrales, W. J. Weber, A. Chartier, and C. Meis, Nucl. Instrum. Methods Phys. Res. B **250**, 46 (2006).
[78] J. Du, R. Devanathan, L. R. Corrales, W. J. Weber, and A. N. Cormack, Phys. Rev. B **74**, 214204 (2006).
[79] M. Zhang, E. K. H. Salje, U. Bismayer, L. A. Groat, and T. Malcherek, Am. Mineral. **87**, 882 (2002).
[80] M. Zhang, L. A. Boatner, E. K. H. Salje, S. Honda, and R. C. Ewing, Am. Mineral. (to be published).
[81] M. Zhang and E. K. H. Salje, J. Phys.: Condens. Matter **13**, 3057 (2001).
[82] A. Deutsch and U. Schärer, Geochim. Cosmochim. Acta **54**, 3427 (1990).
[83] B. P. Glass, S. Liu, and P. B. Leavens, Am. Mineral. **87**, 562 (2002).
[84] P. Dawson, M. M. Hargreave, and G. F. Wilkinson, J. Phys. C **4**,

240 (1971).
[85] M. Zhang, E. K. H. Salje, R. C. Ewing, I. Farnan, S. Ríos, J. Schlüter, and P. Leggo, J. Phys.: Condens. Matter **12**, 5189 (2000).
[86] M. Zhang, E. K. H. Salje, A. H. Wang, X. J. Li, C. S. Xie, S. A. T. Redfern, and R. X. Li, J. Phys.: Condens. Matter **17**, 6363 (2005).
[87] R. M. Almeida, Phys. Rev. B **45**, 161 (1992).
[88] E. I. Kamitsos, A. P. Patsis, and G. Kordas, Phys. Rev. B **48**, 12499 (1993).
[89] T. Furukawa, S. A. Brawer, and W. B. White, J. Am. Ceram. Soc. **62**, 351 (1979).
[90] R. W. G. Syme, D. Lockwood, and H. J. Kerr, J. Phys. C **10**, 1335 (1977).
[91] P. W. O. Hoskin and K. R. Rodgers, Eur. J. Solid State Inorg. Chem. **33**, 1111 (1996).
[92] R. A. Kolesov, C. A. Geiger, and T. Armbruster, Eur. J. Mineral. **13**, 939 (2001).
[93] F. X. Liu, J. L. Yang, and T. P. Zhao, Phys. Rev. B **55**, 8847 (1997).
[94] G. G. Siu, M. J. Stokes, and Y. L. Liu, Phys. Rev. B **59**, 3173 (1999).
[95] T. Hirata, E. Asari, and M. Kitajima, J. Solid State Chem. **110**, 201 (1994).
[96] M. Zhang, E. K. H. Salje, G. C. Capitani, H. Leroux, A. M. Clark, J. Schlüter, and R. C. Ewing, J. Phys.: Condens. Matter **12**, 3131 (2000).
[97] A. Reid and A. E. Ringwood, Earth Planet. Sci. Lett. **6**, 205 (1969).
[98] L. G. Liu, Earth Planet. Sci. Lett. **44**, 390 (1979).
[99] A. Gucsik, M. Zhang, C. Koeberl, E. K. H. Salje, S. A. T. Redfern, and J. M. Pruneda, Miner. Mag. **68**, 801 (2004).
[100] U. A. Glasmacher, M. Lang, H. Keppler, F. Langenhorst, R. Neumann, D. Schardt, C. Trautmann, and G. A. Wagner, Phys. Rev. Lett. **96**, 195701 (2006).
[101] W. van Westrenen, M. R. Frank, J. M. Hanchar, Y. W. Fei, R. J. Finch, and C. S. Zha, Am. Mineral. **89**, 197 (2004).
[102] L. Burgio, R. J. H. Clark, and S. Firth, Analyst (Cambridge, U.K.) **126**, 222 (2001).
[103] B. C. Sales, J. O. Ramey, J. C. McCallum, and L. A. Boatner, J. Non-Cryst. Solids **126**, 179 (1990).
[104] F. Farges, R. C. Ewing, and G. E. Brown Jr., J. Mater. Res. **8**, 1983 (1993).
[105] W. C. Butterman and W. R. Foster, Am. Mineral. **52**, 880 (1967).
[106] E. B. Watson, D. J. Cherniak, J. M. Hanchar, T. M. Harrison, and D. A. Wark, Chem. Geol. **141**, 19 (1997).
[107] F. Fayon, C. Landron, K. Sakurai, C. Bessada, and D. Massiot, J. Non-Cryst. Solids **243**, 39 (1999).
[108] E. Balan, D. R. Neuville, P. Trocellier, E. Fritsch, J.-P. Muller, and G. Calas, Am. Mineral. **86**, 1025 (2001).
[109] T. Geisler, R. T. Pidgeon, W. van Bronswijk, and R. Pleysier, Eur. J. Mineral. **13**, 1163 (2001).
[110] T. Geisler, Phys. Chem. Miner. **29**, 420 (2002).
[111] L. Nasdala, P. W. Reiners, J. I. Garver, A. K. Kennedy, R. A. Stern, E. Balan, and R. Wirth, Am. Mineral. **89**, 219 (2004).
[112] S. Baroni, S. de Gironcoli, A. D. Corso, and P. Giannozzi, Rev. Mod. Phys. **73**, 515 (2001).
[113] E. K. H. Salje and M. Zhang, J. Phys.: Condens. Matter **18**, L277 (2006).
[114] S. Ríos, T. Malcherek, E. K. H. Salje, and C. Domeneghetti, Acta Crystallogr., Sect. B: Struct. Sci. **56**, 947 (2000).
[115] S. G. Kim, H. Asahi, M. Seta, S. Emura, H. Watanabe, S. Gonda, and H. Tanoue, J. Appl. Phys. **74**, 2300 (1993).
[116] X. Huang, F. Ninio, L. J. Brown, and S. Prawer, J. Appl. Phys. **77**, 5910 (1995).
[117] H. Katsumata, S. I. Uekusa, and H. Sai, J. Appl. Phys. **80**, 2383 (1996).
[118] I. D. Desnica-Franković, J. Appl. Phys. **85**, 7587 (1999).
[119] B. C. Johnson and J. C. McCallum, J. Appl. Phys. **95**, 1096 (2004).